MONITORING RICE CROP VARIETIES THROUGH REMOTE SENSING TECHNIQUES

AKBAR YAVARI SHAHREZA
April, 2014

SUPERVISORS:
Dr. Ali A. Abkar
Dr.Ir. W. Bijker

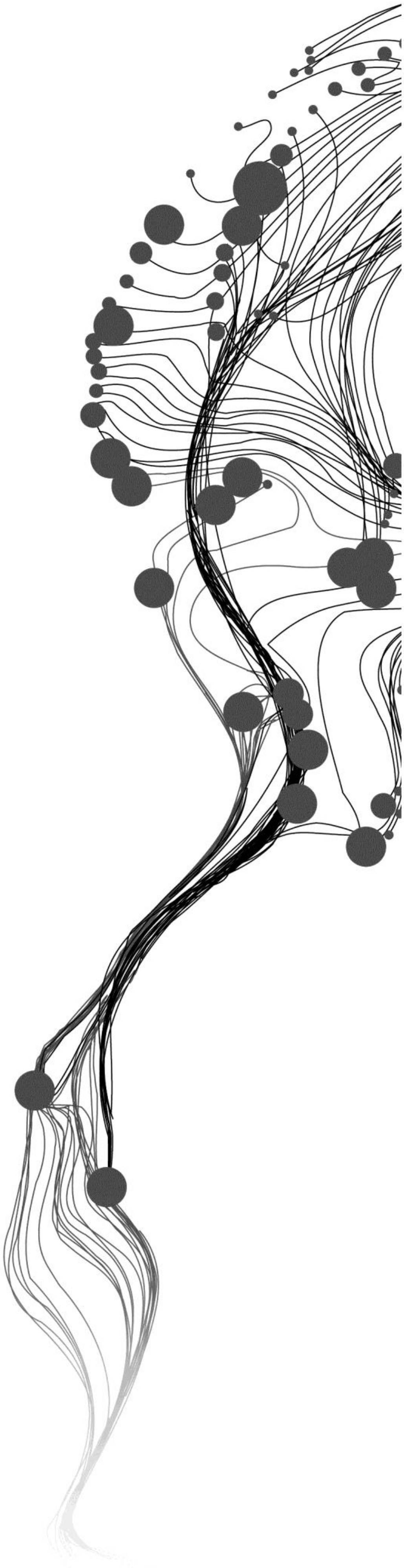

MONITORING RICE CROP VARIETIES THROUGH REMOTE SENSING TECHNIQUES

AKBAR YAVARI SHAHREZA
Enschede, The Netherlands, April, 2014

Thesis submitted to the Faculty of Geo-Information Science and Earth Observation of the University of Twente in partial fulfilment of the requirements for the degree of Master of Science in Geo-information Science and Earth Observation.
Specialization: Geoinformatics

SUPERVISORS:
Dr. Ali A. Abkar
Dr.Ir. W. Bijker

THESIS ASSESSMENT BOARD:
Prof. G. Vosselman (Chair)
Dr. M.R. Sahebi (External Examiner, KNT University)

ABSTRACT

Rice (after wheat) is second important crop in the Iranian diet. According to FAO (2013) Iran was ranked 20th in rice production in the world in 2011 with 3.2 million metric tons. Generally rice is grown in the Caspian areas (Southern shores of the Caspian Sea) of Iran. Although 80 percent of the total rice paddies in Iran are still under local varieties, because of the high quality of these varieties, High Yielding Varieties (HYVs) have been developed at some part of Rasht and Amol in the north of Iran (Shobha Rani, 1998). Actually, because of the higher demand for local varieties in Iran, these two rice types also have differences in terms of marketing, which makes it important to differentiate them when mapping and monitoring rice area.

Newly launched Landsat 8 provides freely available multi-temporal images. Landsat 8 products have an improved signal-to-noise (SNR) radiometric performance which will enable improved land cover mapping.

This research aims at investigating the monitoring of rice crop varieties with these Landsat 8 products. In other words, classifying Landsat 8 images into two rice varsities is challenging. These classes have similar spectral properties with small patches of paddy rice fields in the study area. Images are selected based on the local rice crop calendar and the cloud cover condition. First the images segmented to create homogenous objects to extract segments feature. This segmentation part helps to group the pixels of the same varieties rice fields which their spectral values affected by weather condition or diseases of rice crop. The calculated features are Normal Difference Vegetation Index (NDVI), Land Surface Water Index (LSWI), Brightness and mean value of the spectral bands. The extracted feature divided into two sets: 1- LSWI, NDVI and brightness (10 bands) 2- mean spectral values (18 bands). Field samples were collected at the same time of image acquisition and used as training samples in the Random Forest (RF) and Support Vector Machine (SVM) classification methods. Both classification methods (SVM, RF) were implemented for each feature bands set. The classification was done in pixel level. The overall accuracy for SVM is 95.2% for 10 feature bands and 92.4% for 28 feature bands. The overall accuracy for 10 bands and 28 bands in RF are 94.9% and 88.5% respectively. The results show the possibility of discriminating and classifying two main rice varieties in the study area with multi-temporal Landsat 8 images. Improving the classification results and testing different algorithm to find optimum parameter for segmentation and classification could be part of future work.

Keywords: Iranian rice crop varieties, image classification, image segmentation, Landsat 8, multi-temporal satellite image

ACKNOWLEDGEMENTS

I would like to express my very great appreciation to my first supervisor Dr. Ali Abkar for his valuable and kind support and suggestions during this project. I want to extend my special gratefulness to my second supervisor Dr. Wietske Bijker for her critical comments and advices during this research in the Netherlands and after that.

I express my special thanks to my dear friends for their emotional support that was a big help for me to come over the difficulties and problems during this work.

Finally, my dear mother and father, your kind support is the reason that I am standing here. Thank you for all you have done for me.

TABLE OF CONTENTS

LIST OF FIGURES

LIST OF TABLES

1. INTRODUCTION

1.1. Motivation and problem statement

Nowadays, one of the most important problems which people all around the world are facing is the population growth and subsequently food demand issues. According to Thi Thu Ha (2013), the Agriculture Organization of the United Nations (FAO) has predicted that there will be a need to increase overall food production by 70% for feeding 9.1 billion world populations in 2050. Rice, together with wheat and maize, is one of the three agricultural crops which are used as food by almost half people of the world. World rice production has risen from almost 200 million tons in 1960 to over 678 million tons in 2009 (Thi Thu Ha, 2013). This growth happened mostly because of the so called "Green Revolution".

Green Revolution is a project with a number of researches, development and technology transfer innovations in agricultural field worldwide. This project was started to increase agriculture production by development of irrigation infrastructure, modernization of management techniques and also development of high-yielding varieties (HYV) of cereal grains (Hazell, 2009). Green Revolution especially focused on rice and wheat, as two main agriculture crops in the World, and lead to production of improved varieties of these crops.

Rice (after wheat) is second important crop in the Iranian diet (Darvishsefat et al., 2011). According to FAO (2013) Iran was ranked 20th in rice production in the world in 2011 with 3.2 million metric tons. Generally rice is grown in the Caspian areas of Iran. Production is mainly concentrated along the Caspian Sea provinces (Gilan, Mazandaran and Golestan provinces) and around 500,000 hectare of the south of Caspian Sea is covered by rice. Although 80 percent of the total rice paddies in Iran are still under local varieties, because of the high quality of these varieties, HYVs have been developed at some part of Rasht and Amol in the north of Iran (Shobha Rani, 1998).

Improved rice varieties have higher yield per hectare, more resistance to blast, physical and phenological differences compared to local varieties. Shorter stature, denser canopy, different in managing practices (e.g. time of planting, fertilizing, etc.) and different time of growth duration and harvesting are examples of physical and phenological differences of improved varieties. Actually, because of the higher demand for local varieties in Iran, these two rice type also have differences in terms of marketing.

Due to rice varieties differences, there is a growing need for more detailed and precise information about rice varieties in the world. This information could be useful for agricultural decision makers, food security managers and even insurance companies for overall production per hectare assessment, damage assessment after disease and etc. However, finding a cost effective and fast approach to control and monitor the agriculture areas and especially rice paddies was a big issue till remote sensing technologies have been implemented (Van Niel et al., 2004).

Development of remote sensing technologies has led to increasing availability of temporal satellite images (Petitjean et al., 2012a). Landsat with good land coverage provides cost free temporal images. Landsat 8, launched on February 2013, images the entire Earth every 16 days. Images consist of two thermal bands and nine spectral bands with a spatial resolution of 30 meters for bands 1 to 7 and 9. Spatial resolution of band 8 (panchromatic) is 15 meters. Landsat 8 sensors provide improved signal-to-noise (SNR) radiometric performance which will enabled improved land cover mapping (USGS, 2013).

1.2. Research identification

1.2.1. Research objective

The objective of this research is to discriminate and classify traditional and high yielding rice varieties at regional level in the study area using multi-temporal Landsat 8 images and local knowledge about area and varieties.

1.2.2. Research questions

To reach the research objective, the research questions could be formulated as follows:

1. Is it possible to classify traditional and high yielding rice varieties in the study area by use of multi-temporal satellite images?
2. How can local knowledge and additional information (e.g. crop calendar) be included in the multi-temporal image classification?
3. Are Landsat 8 images proper (spectrally and spatially) to classify two main rice varieties in the regional level in the study area?

1.2.3. Innovation aimed at

The novelty of this research could be divided into three parts:

- Using multi-temporal satellite images to classify rice crop at cultivar level (two main varieties) instead of crop level.
- Using images of the recently launched Landsat 8 with improved radiometric characteristics compared to previous one.
- The way that local knowledge is included into multi-temporal satellite image analysing.

1.3. Research approach

Different temporal behaviour of rice varieties in the study area and existence of additional information about those varieties is the reason that Object-based analysing of multi-temporal satellite images is used in this research. Multi-temporal Landsat 8 images of 2013 are used in this research to classify traditional rice varieties, and high yielding varieties.

The method of this research could be divided into four main steps:

1- Preprocessing of Landsat 8 images (georeferencing and atmospheric correction)
2- Segmenting each image and feature extraction
3- Analysing and classifying multi-temporal segmented image
4- Accuracy assessment

Research has been done on three cloud free images, one at the start of the cultivation period another one at the middle of the growth stage and the third one is almost end of the growth stage.

The below Figure shows the research flowchart:

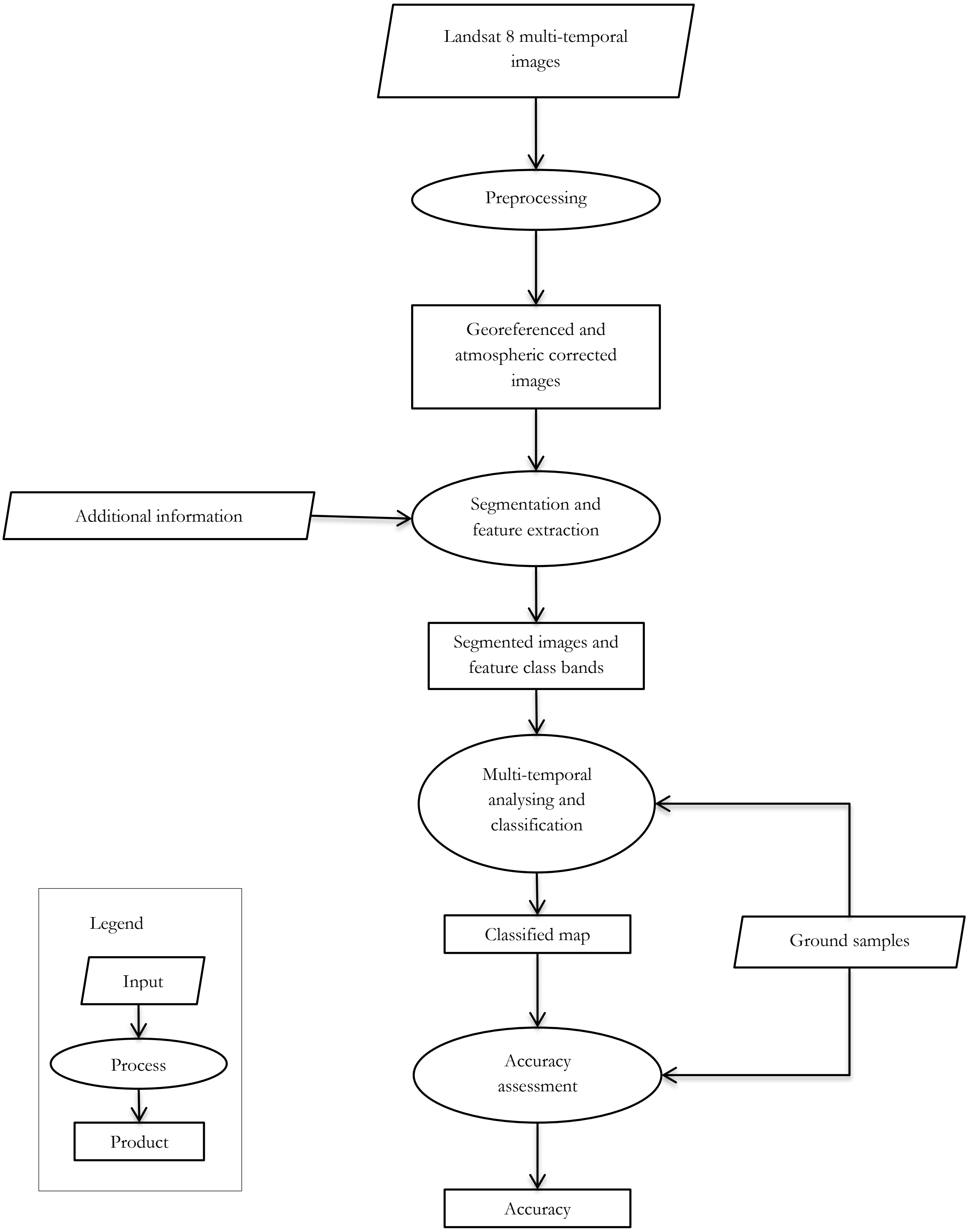

Figure 1-1: Proposed research approach

1.4. Literature review

The time dimension must be taken into account in the classification algorithm when the classes of interest have differences in temporal behaviour (e.g. agronomical fields). According to Petitjean et al. (2012a) the use of time dimension is divided into three main categories: time as identifier, pairwise time ordering and time ordering the sequence. Authors developed a method to analyse satellite image time series (SITS) by use of dynamic time warping (DTW). The major problem of DTW is its calculation complexity. Niennattrakul et al. (2012) presented a template matching framework to reduce the DTW computational requirements.

Petitjean et al. (2012b) proposed spatio-temporal reasoning to classify time series images. The underlying idea is to start with segmenting each image of a time series. The spatial information is considered in this part. Then, characterizing each region by computing different features (e.g. smoothness, area of region, compactness etc.). In the next step each pixel of the image is characterized by a number of features, region-associated features and directly sensed radiometric values ("enriched" pixels). Then SITS methods are implemented to analyse and classify time series images which have these "enriched" pixels. The authors implemented this new method for classifying different crop types in an agronomical area.

Zhou et al. (2008) presented an object-based approach to analyse the urban landscape at the parcel level. They used high-resolution aerial imagery and light detection and ranging (LIDAR) data. Authors used additional spatial information including boundaries and property parcel to simplify segmentation and improve classification accuracy. Drăgut et al. (2010) presented a technique to estimate the scale parameter in object-based image analysing.

With a quick look at the most of the studies about crop fields, it is clear that the majority of them are about classifying images at the crop level to estimate the cultivated area or for damage assessment. Nuarsa et al. (2010) used multi-temporal Landsat ETM+ to map the distribution of rice fields. They developed a new index named RGVI (rice growth vegetation index). The authors used this index to estimate the rice cultivation area and rice crop age. Savin et al. (2009) used Landsat images to extract the rice fields the estimate the production of the rice by use of NDVI in MODIS images from 10 continuous days.

At the cultivar level, Breunig et al. (2011) worked on soybean varieties classification. They evaluated four different classification techniques to discreminate soybean varieties. In other research Shao et al. (2001) used Radarsat images to estimate rice production in China. They produced a rice type distribution map which shows four rice types with different life span.

One of the unique features of rice paddies is that rice is grown in the flooded fields. Xiao et al. (2002) used multi temporal VEGETATION (VGT) sensor images to evaluate the normalized difference water index (NDWI) for describing spatial and temporal changes of surface moisture. The authors compared temporal and spatial dynamics of normalized difference vegetation index (NDVI) and NDWI. They found that NDWI has enough sensitivity to detect the surface water increase of the flooded rice fields.

To identify changes in the rice fields that are a mixture of water surface and green canopy, vegetation indices which are sensitive to both water and vegetation are required. Xiao et al. (2005) developed an algorithm to map rice paddies based on the sensitivity of land surface water index (LSWI). The authors used the MODIS images to produce time series of three vegetation indeces (LSWI, EVI and NDVI) to identify the transplanting and flooding time in the rice fields for rice mapping.

In the recent years modern inteligent techniques have a significant roll in image classification. Artificial Neural Networks (ANN), Support Vector Machines (SVMs) and Decision Trees (DT) are some of these inteligent techniques. In a DT, each node tests the feature value and branches shows the test output and leaves represent the classes or class distribution (Han et al., 2006). Decision trees have interpretable rules with fast calculation as well as the capability of feature selection (Wang et al., 2008).

Wu et al. (2009) used decision trees classifier for urban land use classification by using a combination of LIDAR data and GIS information. In another research Garcia-Gutierrez et al. (2011) used DT and

LIDAR data to classify land use in mixed-land zone (the mix of different land uses i.e. manmade sites, industrial areas, roads and railways with the natural areas like forrest and vegitation) automaticaly.

Many studies have used SVM as a new machine learning method for land use classification (Bilgin et al., 2011; Foody et al., 2004; Huang et al., 2002; Li et al., 2012; Melgani et al., 2004; Rabe et al., 2010). In those studies SVM classifier showed more accurate results than the other alghorithms. Due to satisfactory performance of the SVM many researchers perefer to use this method in the classification. Moustakidis et al. (2012) proposed a SVM-based fuzzy DT for the land use classification. The authors tested this approach on QuickBird multispectral images for natural forest classification and hyperspectral data for urban classification. Although SVM classifiers are used in many studies, it is difficult and time consuming to determine required parameters (Mountrakis et al., 2011).

2. STUDY AREA AND MATERIALS

2.1. Study area

Sari is the provincial capital of Mazandaran, located in the north of Iran, between the northern slopes of the Alborz Mountains and southern coast of the Caspian Sea. At the 2006 census, its population was 259,084, in 71,522 families. The study area is located near the Sari and includes Fajr, Hybrid, Khazar, Nemat, Neda, Shiroudi and Tarom varieties. Tarom, originally from Mazandaran, is considered to be one of the best and highest quality local varieties. Khazar originated from Gilan Province but is also cultivated in Mazandaran due to its high yield and adaptation to Mazandaran climate. Grain texture is chalky and the colour is dark cream resembling various Sadri types especially Tarom. Hybrid, a modified variety, has an increased yield of 20–25% as compared with the original varieties. Neda and Nemat are also high yielding ones. The paddy is sown in April in a nursery. Transplanting takes place about forty days later (May-June), which allows the time necessary to prepare the fields for paddy.

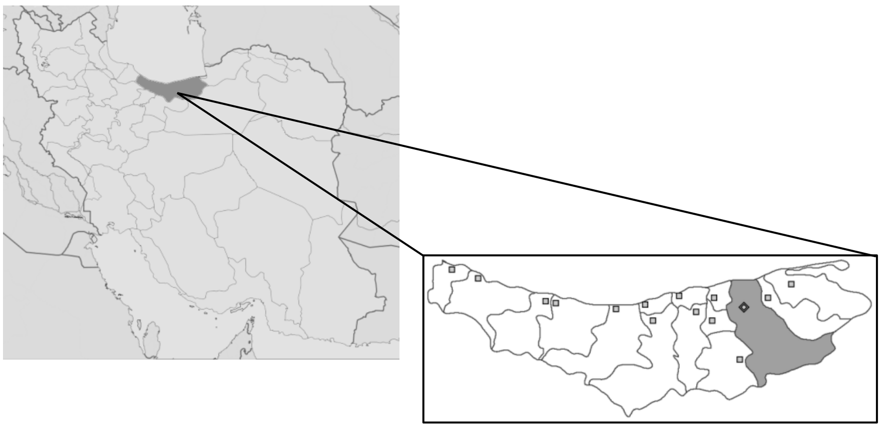

Figure 2-1: Location of the Sari in the Mazandaran province

2.2. Satellite data

In this research Landsat 8 satellite images are used. The objective of the Landsat mission is to enables global studies of the Earth's surface changes. The collection of multispectral moderate resolution images of the Earth began in 1972 with the launch of the first Landsat (Micijevic et al., 2011). The Landsat images are used in agricultural research for change detection, analysing the health and vigour of crops over the growing season, forecasting crop production and monitoring drought.

The Landsat 8 launched on 11^{th} February 2013. It carries two sensors named Operational Land Imager (OLI) and Thermal Infrared Sensor (TIRS). The radiometric resolution of the sensors are 16-bit with an improved signal to noise radiometric performance which enables better characterization of land cover mapping (USGS, 2013). The images have 9 spectral bands with 30 meter spatial resolution for bands 1 to 7 and 9. Band 8 is panchromatic band with 15 meter spatial resolution. Two thermal bands have 100 meter spatial resolution which is resampled to 30 meters to match OLI multispectral bands.

Table 1 shows the characteristics of Landsat 8 OLI and TIRS bands and Figure 2-2 shows the differences between Landsat 8 and Landsat 7 ETM+ bands.

Table 1: Landsat 8 bands charachteristics (USGS, 2013)

Bands	Wavelength (micrometer)	Resolution (meter)
Band 1 – coastal aerosol	0.43 – 0.45	30
Band 2 – blue	0.45 – 0.51	30
Band 3 – green	0.53 – 0.59	30
Band 4 – red	0.64 – 0.67	30
Band 5 – near infrared (NIR)	0.85 – 0.88	30
Band 6 – shortwave infrared (SWIR) 1	1.57 – 1.67	30
Band 7 – shortwave infrared (SWIR) 2	2.11 – 2.29	30
Band 8 – panchromatic	0.50 – 0.68	15
Band 9 – cirrus	1.36 – 1.38	30
Band 10 – thermal infrared (TIRS) 1	10.60 – 11.19	100
Band 11 – thermal infrared (TIRS) 2	11.50 – 12.51	100

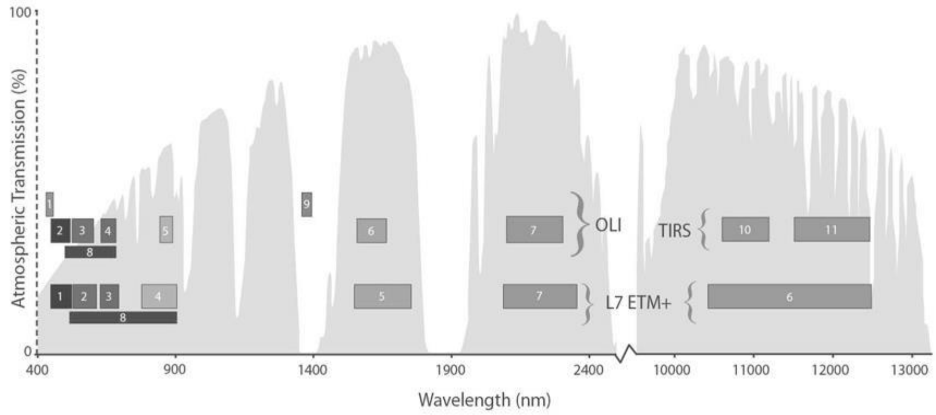

Figure 2-2: Landsat 8 bands versus Landsat 7 ETM
(USGS, 2013)

Landsat 8 images are provided in Standard Terrain Correction (level 1T). This level provides systematic radiometric and geometric accuracy by use of ground control points. The images are georeferenced and provided accuracy in this level is 12 meter circular error with 90% confidence level for OLI and 41 meter circular error with 90% confidence level for TIRS.
Table 2 shows data characteristics of Landsat 8 data products.

Table 2: Landsat 8 data product characteristics (USGS, 2013)

Data format	**GeoTIFF**
Resampling method	Cubic Convolution
Map projection	Universal Transverse Mercator (UTM)
Datum	World Geodetic System (WGS) 84
Image orientation	MAP (North-up)

The Landsat 8 revisit time is 16 days with an 8-day offset from Landsat 7.
According to the rice crop calendar in the study area, which is shown in Table 3 for three different rice type, the satellite images downloaded from USGS web site for this research.
Table 3 shows the nursery preparation, transplanting and harvesting time of three rice varieties: Early maturing (such as Tarom), Mid-term varieties (such as Shiroudi) and Late maturing. All the information of these two tables (Table 3 and Table 4) is collected by help of the Iranian rice research institute experts.

Table 3: Rice crop calendar in the study area

Rice cultivars	Nursery preparation	Transplanting	Harvesting
Early maturing (short duration varieties)	21st March to 21st April	21st April to 21st May	1st August to 23rd August
Mid-term varieties	30th March to 30th April	30th April to 31st May	23rd August to 22nd September
Late maturing	21st March to 21st April	21st April to 10th May	6th September to 23rd September

Table 4 shows the satellite images date of acquisition and rice cultivars growth stage. This table also shows the cloud cover condition of each satellite image.

Table 4: Date of satellite image acquisition and rice cultivars growth stage

Image date of acquisition	Tarom growth stage (Early maturing)	Shiroudi growth stage (Mid-term varieties)	Image cloud cover condition
11th May	First of Tillering	First of Tillering	Partly cloudy
27th May	Middle of Tillering	First of Tillering	No-cloud
12th June	End of Tillering and start of reproductive stage	End of Tillering	Partly cloudy
28th June	Booting	End of Tillering and start of reproductive stage	Partly cloudy
14th July	Start of Heading	Booting	No-cloud
30th July	Start of ripening stage	Start of Heading	Partly cloudy
15th August	Harvesting	Start of ripening stage	No-cloud
31st August	-	Harvesting	Cloudy

2.3. Field data

Based on the field survey the majority of the fields in the study area are planted with Tarom as the traditional variety and Shiroudi as the high yielding variety for this year. The field data are polygons that were collected by use of a handheld GPS at the same time of acquisition of the satellite images. The class of each polygon is collected by direct survey with the farmers and rice experts of the rice research institute.
These ground samples are divided into two parts, one part for training samples and the other part for validation. A small polygon of the middle of each sample is selected for training samples and the whole of the pixels in the polygon is used for validation.

Figure 2-3 shows the location of the field data on the pansharpend image of 27th May. Figure 2-4 shows the selected polygons for training and test samples. Pansharpend image is just used here for better visualisation and not in the implemented method.

2.4. Software

For this research the pre-processing and mathematical computation is done with MATLAB software. ENVI as a geospatial image analysis software is used for the classification and extracting subsets of area of interest.

eCognition Developer is a development environment for object-based image analysis which is used to develop rule sets for the remote sensing data analysis. In this research image segmentation and feature extraction is done by this software. This software is provided by KNT University for this research.

ArcGIS is a GIS software which is developed by ESRI and it has spatial analyst tools that is used in this research.

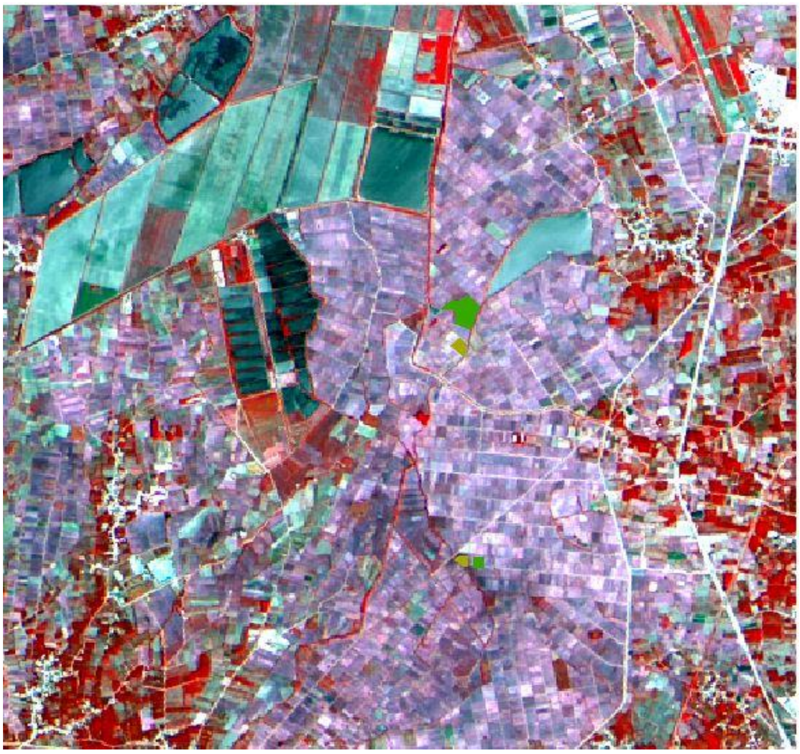

Figure 2-3: Location of the collected field data on Pansharpend image of 27th May

The polygons of two classes of rice (Tarom and Shiroudi) collected by GPS are shown in green and dark yellow

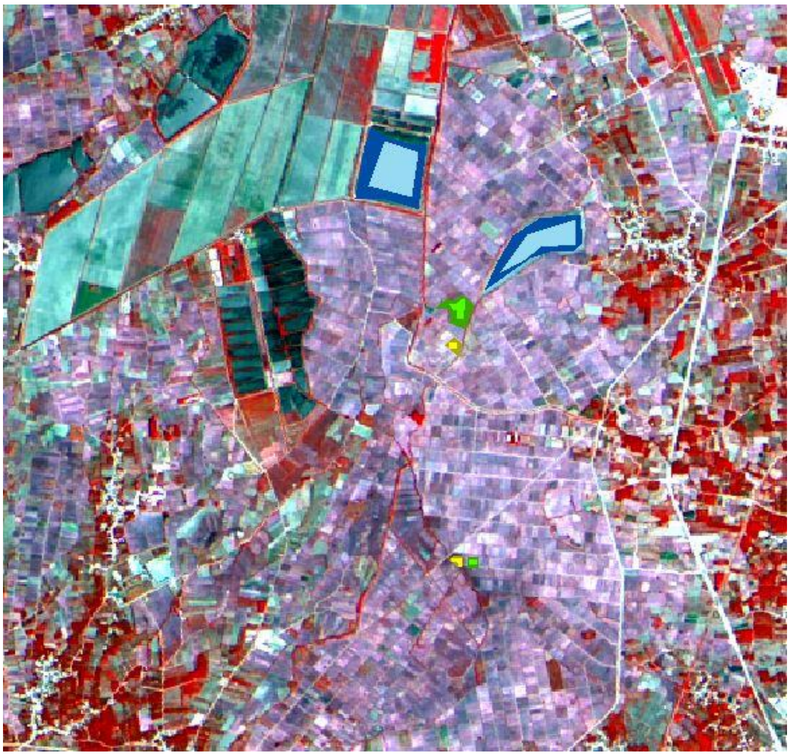

Figure 2-4: Training and test polygons of three classes in Pansharpen image of 27th May

Two classes of rice are shown in dark green and dark yellow, one class of water are shown in dark blue. The smaller polygons with light colours on top of each dark polygon show the selected training sets.

3. THEORITICAL FOUNDATION

3.1. Landsat 8 pre-processing

Landsat 8 data products consist of quantized and calibrated scaled Digital Numbers (DN) which represents multispectral data acquired by OLI and TIRS and delivered in 16-bit unsigned integer. These data can be converted to Top Of Atmosphere (TOA) reflectance or radiance.
The required coefficients for these conversions are provided in a MTL file which is available with each image (U.S. Geological Survey, 2013).

3.1.1. Conversion to TOA Radiance

$$L_\lambda = M_L * Q_{cal} + A_L$$

Where:
L_λ= TOA spectral radiance (Watts/(m2 * srad * µm))
M_L= Band-specific multiplicative rescaling factor
A_L= Band-specific additive rescaling
Q_{cal}= Quantized and calibrated standard product pixel values (DN)

3.1.2. Conversion to TOA Reflectance

TOA planetary reflectance, without correction for solar angle:

$$\rho\lambda' = M_\rho * Q_{cal} + A_\rho$$

Where:
$\rho\lambda'$= TOA planetary reflectance, without correction for solar angle.
M_ρ= Band-specific multiplicative rescaling
A_ρ= Band-specific additive rescaling factor
Q_{cal}= Quantized and calibrated standard product pixel values (DN)

TOA reflectance with a correction for the sun angle:

$$\rho\lambda = \frac{\rho\lambda'}{\cos\theta_{SZ}} = \frac{\rho\lambda'}{\sin\theta_{SE}}$$

Where:
$\rho\lambda$ = TOA planetary reflectance
θ_{SE}= Local sun elevation angle
θ_{SZ}= Local solar zenith angle; θSZ = 90° - θSE

According to U.S. Geological Survey (2013), solar exoatmospheric spectral irradiances (ESUN) values are not provided for Landsat 8 because they are not required for converting DN values to TOA reflectance.

3.2. Segmentation and feature extraction

Image segmentation is the first step in object-based image analysis. Finding the best scale parameter to do segmentation is the crucial part. Scale parameter is a measure to control the degree of heterogeneity within an image object (Drăgut et al., 2010). Smith (2010) used Random Forest (RF) to optimize image segmentation parameters including scale parameter. Nikfar et al. (2012) used a genetic algorithm for scale parameter optimization.

Drăgut et al. (2010) presented a technique for scale parameter estimation in eCognition software. Estimation of Scale Parameter (ESP) is the tool which is proposed by these authors. This tool is based on the idea of local variance of object incongruity within a scene.

3.3. Random Forest classification method

Bootstrap aggregation (bagging) predictor is an aggregated predictor. Bagging is used in statistical classification and regression for avoiding over fitting by reducing variance. It starts with selecting random subsets from training samples and in the next step it constructs decision trees for each subset and find a label for the input samples based on the results of DTs. It repeats these two steps and assigns the class with the higher repetition number to the input sample. Boosting assigns the same weight for all classes in the first step. In the next iterations, it use weighted classes instead of sampling and assigns low weight to the classes that are trained correctly and high weight to the class that are trained wrongly. In this method the samples are selected from the existing classes with different weights. The underlying idea is that in each step classes which are not classified correctly with previous samples have the higher weights for next iteration (Breiman, 1996).

RF classifier which has been developed by Breiman (2001) is one of the other ensemble classification methods. RF is a combination of DTs $\{DT(x, \theta_k)\}_{k=1}^{T}$ where θ_k is a random vector that is selected freely but with the same distribution with $\theta_1, \ldots, \theta_{k-1}$. x is the input vector. In this method, first a number of independent DTs is grown and each tree decides about the class label separately. At the end classification output is generated by the class with the majority of votes of all individual trees (Jin, 2012).

This method is not influenced by the number of training samples and it works fast in hyperspectral images. Avoiding over fitting is another advantage of this method. Several studies have demonstrated the advantage of RF in land cover classification (Gislason et al., 2006; Pal, 2005; Smith, 2010). Figure 3-1 shows the RF classification workflow (Guo et al., 2011).

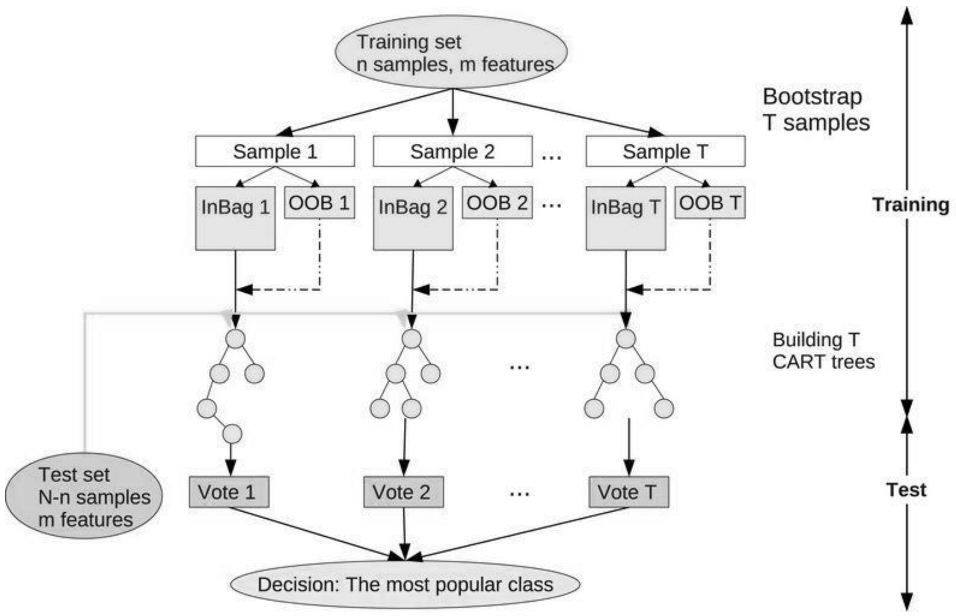

Figure 3-1: Random Forest classification workflow

(Guo et al., 2011)

RF algorithm has the following steps:

- Two parameters must be specified. T, the number of trees, and M, the number of random subsets of features. The larger the size of M, the higher the correlation between the trees and the larger the strength (classification accuracy) of individual tree (Jin, 2012).
- In this step a subset of input samples is selected randomly to use for accuracy assessment of each tree. These data are called Out-of-bag (OBB) data. OBB data are used to calculate total OBB error rate. This error is unbiased and could be used to plot relation between OBB error and number of trees (Breiman, 2001).
- In this step each tree makes the decision on the class independently.
- The results of all the trees will be combined and the class with the majority of votes will be assigned to the input sample.

3.4. Support Vector Machine

SVM is a non-parametric classification method derived from statistical learning theory aims to drawing a separate hyperplane between classes in feature space (Wu et al., 2004). Hsu et al. (2003) noted that SVM provides good classification results from noisy data. Many studies show the performance of SVM in multi-source data classification even with small sample datasets (Dalponte et al., 2008; Jones et al., 2010; Salah et al., 2010).

SVM separates the classes using a decision surface that maximize the distance between classes in the feature space. This surface is often called optimal hyperplane and the data points closest to the hyperplane are called support vectors (Mahour et al., 2012).
For solving the non-linear classification problems Boser et al. (1992) introduced a kernel trick. The most common kernels for SVM classifiers are: linear, Gaussian radial-basis function (RBF), polynomial and sigmoid. RBF is the default kernel which shows good performance in most cases (Mahour et al., 2012). The mathematical representation of RBF kernel is (Hsu et al., 2003):

$$K(x, x_i) = \exp\left(-\frac{\|x - x_i\|^2}{\gamma^2}\right), \gamma > 0$$

Where:

- γ is user-defined kernel parameter
- x is a sample in the original data space
- x_i is an corresponding sample in the feature space

4. IMPLEMENTATION AND RESULTS

4.1. Study area selection and image preproccesing

As it mentioned previously, there was three cloud free Landsat 8 images available for the selected study area. 27th May is almost at the start of rice cultivation in the study area and the fields are flooded, 14th July is at the middle of growth stage and 15th August is almost the end of the growth stage for the endemic varieties but the HYVs (e.g. Shiroudi) is in the ripening stage and not harvested (see Table 4).
Each Landsat 8 images cover 170 KM North-South and 183 KM East-West. For this research, study area includes 223 by 230 pixels of the whole scene. Figure 4-1 shows the three cloud free images in false colour composite (5,6,4) selected for this research. The rice fields have significant changes during these three image dates as it is shown in Figure 4-1.

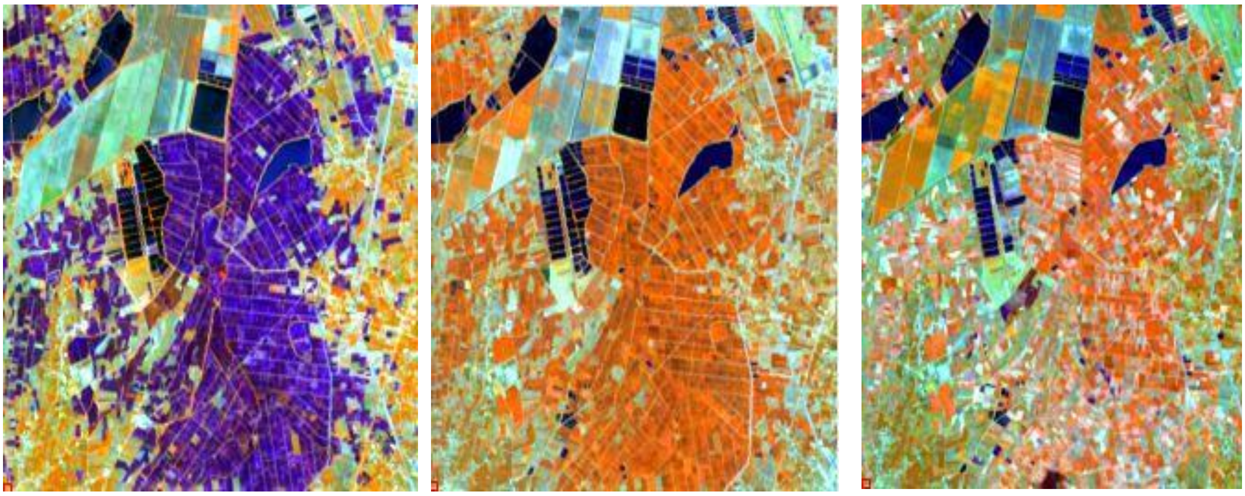

Figure 4-1: Selected spatial subset of three image dates false color composites (RGB= 5, 6, 4)

from left to right: 27th May, 14th July and 15th August

Six bands of each image were selected as a spectral subset of these three images. For this research I did not use band 1 (coastal aerosol) and band 9 (cirrus) because they are more useful in weather researches. Also, the panchromatic band and the thermal bands were omitted.
After the subset was selected, all the 18 bands of these three image dates were converted to TOA reflectance and outputs saved as an 16-bit unsigned integer for the next step.

4.2. Image segmentation and feature extraction

In this step, the ESP tool (see section 3.2) was implemented to optimize the scale parameter. This tool works with one band as input. After the algorithm has been ran, a number of proper scale parameters calculated based on the local variances. In this research, the blue band of the 14th July image date was selected as input and estimated scale parameter was 22, 33, 54 and so on. Some of these estimated scale parameters were used for segmentation and with visual comparison 33 was selected as the final scale parameter. In the selection of final scale parameter, it was tried to have neither small object nor big object based on the homogeneity of the fields which was checked visually. Also, it was tried to have homogeneous recognizable objects (i.e. water bodies) as one object. Segmentation was done for all 18 bands together. Figure 4-2 shows the segmentation result.

Four different features were calculated and extracted for each segment. Extracted features are NDVI, LSWI1, LSWI2 and brightness. Land Surface Water Index (LSWI) was calculated for both SWIR bands of the Landsat 8.

$$LSWI1 = (nir-swir1) / (nir+swir1)$$
$$LSWI2 = (nir-swir2) / (nir+swir2)$$

At the end, 10 feature bands were calculated: 3 NDVI bands, 6 LSWI bands and one brightness band. Also mean of the spectral bands for each segment were calculated in 18 different bands (18 bands).

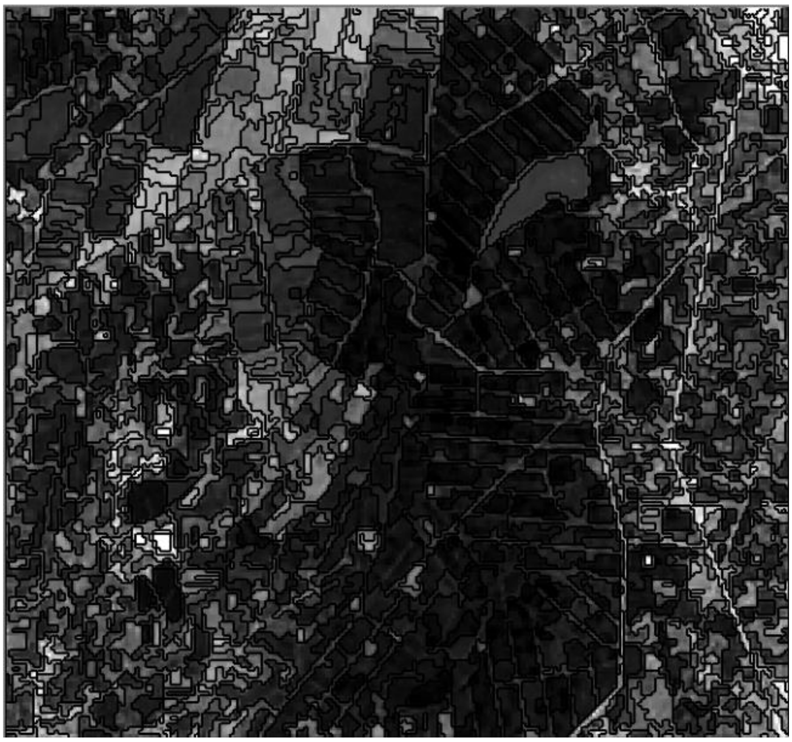

Figure 4-2: Segmentation result, 18 bands of the 3 image dates together

4.3. Classification

After extracting feature bands, all the segmented bands convert to pixel size and the feature values assign to each pixel in each band. Classification was done in pixel level. For the classification two algorithms were used, SVM and RF (see the section 3.3 and 3.4). Classification was done for two set of feature bands: First, images were classified with 10 feature bands (3 NDVI, 6 LSWI and brightness) as input for two classification methods. Results are shown in Figure 4-3.

After that all mean of spectral bands (18 bands) were added to first 10 bands and images were classified with 28 bands as input for two classification methods. Results are shown in Figure 4-4.

Both algorithms were trained with same sample data collected from the field work. As the objective of this research is not focused on the algorithm optimization, all the input parameter was set as default in the software.

In the results, differences outside of the rice area are because there was no accurate information about the No-rice areas and non-rice classes in the study area. To solve the lack of information and better visualisation, a rice mask was generated and applied to the classified maps to mask the No-rice area.

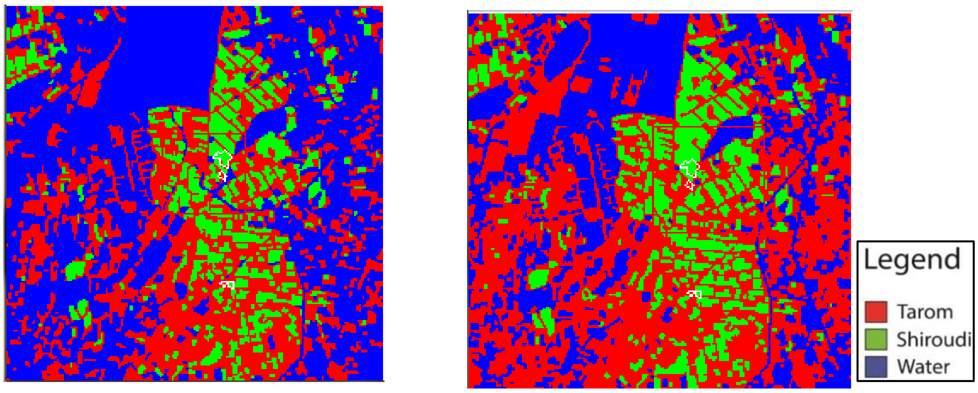

Figure 4-3: Classification results, feature bands are used as inputs

Left: RF result, Right: SVM result

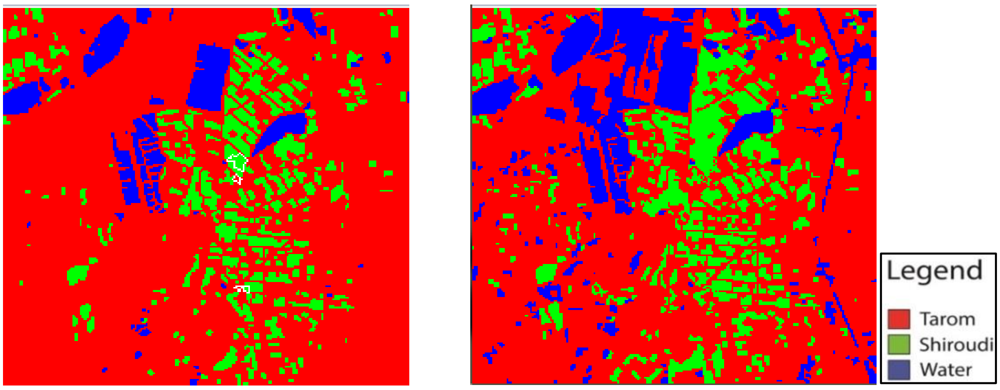

Figure 4-4: Classification results, feature bands plus mean spectral values are used as inputs

Left: RF result, Right: SVM result

4.4. Rice mask

The Rice mask was generated by use of NDVI differences between 27th May and 14th July image date. Rice is cultivated in flooded fields in the study area so in the 27th May image, the rice fields are flooded and have low NDVI. After about two months and at the middle of the growth stage (14th July), rice fields have a significant change in NDVI while the rest of the area (forest, water bodies and other type of agriculture fields) have less changes.

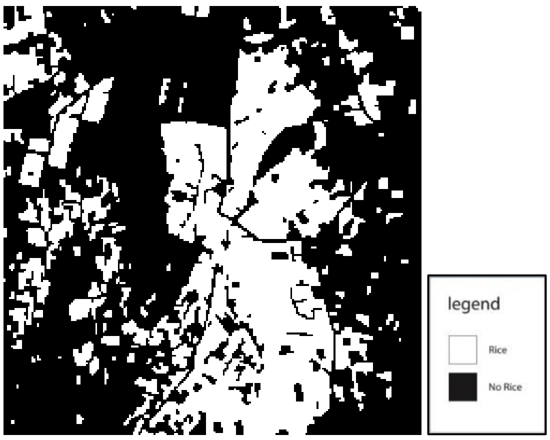

Figure 4-5: Rice mask, generated with NDVI differences of 14th July and 27th May

For this, first the NDVI map of these two image dates was calculated. After that, a difference NDVI map was generated by subtracting the two NDVI maps. At the end a binary map was generated by defining a threshold on the difference NDVI map. The result of this Rice mask generation is shown in Figure 4-5. The Rice mask applied to the classification results to remove no-rice areas for the better interpretation. Figure 4-6 shows the classification results after applying the Rice mask.

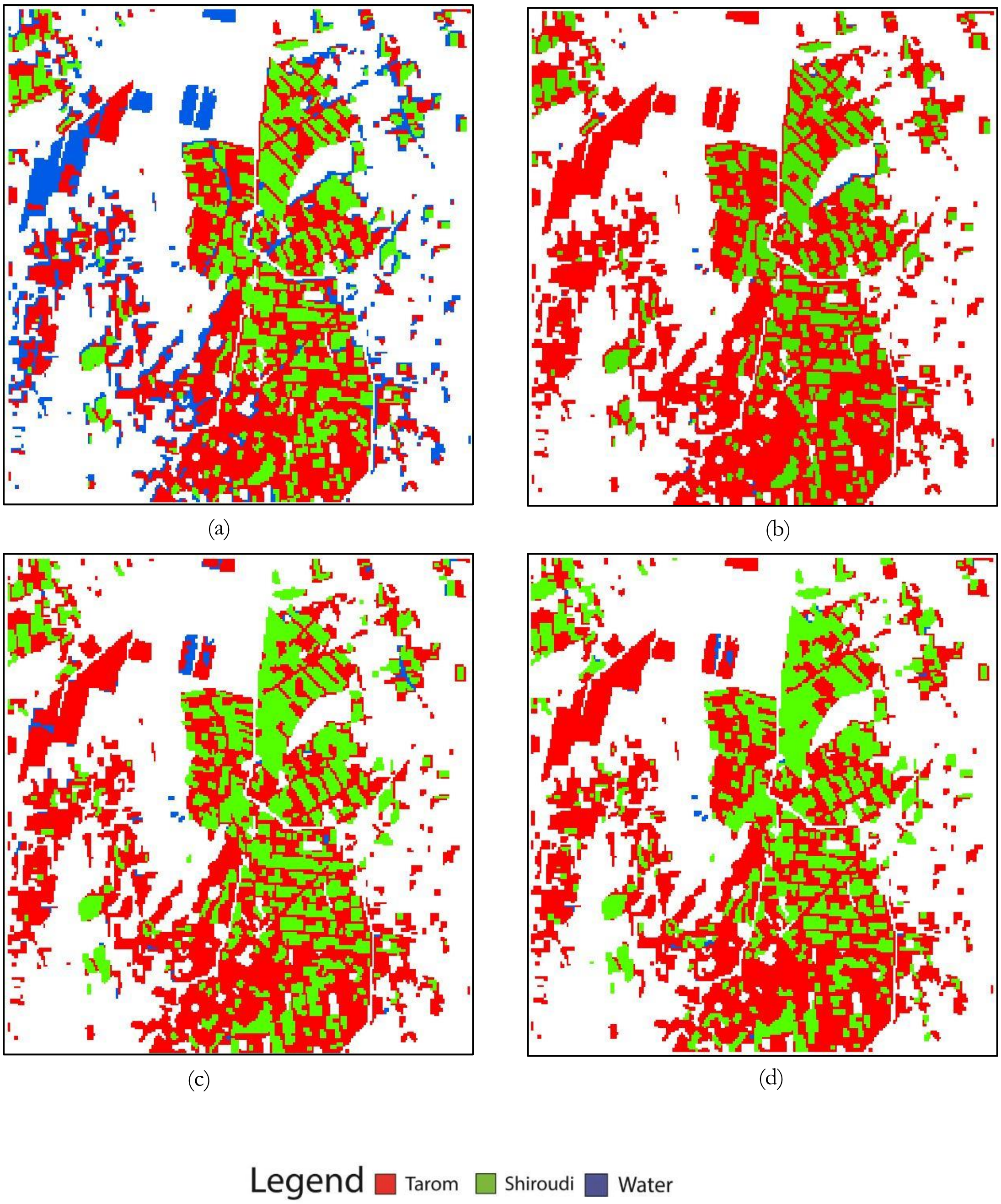

Figure 4-6: Classification maps after the Rice mask has been applied

a) RF, 10 bands b)RF, 28 bands c)SVM, 10 bands d)SVM, 28 bands

4.5. Accuracy assesment

To assess the results of each classification method the kappa coefficient, user accuracy and product accuracy was calculated by use of sample data. Due to the differences in the number of sample data for each class and also low number rice samples (see Table 7) the user/producer accuracy has big differences in each class. Table 5 shows the accuracy assessment of the results.
Table 6 shows the user and producer accuracy of the results for each class in both methods.

Table 5: Accuracy assessment for two implemented classification methods

	SVM		Random Forest	
	10 bands	**28 bands**	**10 bands**	**28 bands**
Kappa	0.8333	0.7546	0.8176	0.6604
Overal acuracy	95.21	92.45	94.92	88.53

Table 6: User and producer accuracy of the classification assessment

		SVM		RF	
		10 bands	**28 bands**	**10 bands**	**28 bands**
Tarom	User Acc. (percent)	41.82	30	39.62	21.65
	Prod. Acc. (percent)	100	91.30	91.30	91.30
Shiroudi	User Acc. (percent)	98.63	96	95.52	95.89
	Prod. Acc. (percent)	96	96	85.33	93.33
Water	User Acc. (percent)	100	100	100	100
	Prod. Acc. (percent)	94.92	92.05	96.28	87.82

5. DISCUSSION

In this chapter the achieved results will be discussed and analysed. First to some extent the quality of the generated Rice mask (See Section 4.4) will be assessed by the visual comparison of this Rice mask with the generated colour composites (CC) of the three image dates. Then the chapter will be followed by classification and spatial error pattern analysis. Also, the separability of the classes in the feature space will be argued. At the end the results of segmentation part will be discussed.

As it was explained in Section 4.4, Rice mask was generated using the NDVI differences of the first two dates of the images. Rice Mask generation could also be generated in an automatic manner in order to optimize the threshold for masking Rice from No-Rice. Due to the lack of accurate information about the classes of No-Rice area (such as Forest, orchards, and other agricultural crops), threshold for generating the Rice mask is selected visually. In fact this could be planned well in advance to collect the required data and/or information during a field visit, for which I didn't have time nor planned in the course of the implementation of the research to do so. Figure 5-1 shows the results of the visual interpretation and that all the water samples are excluded from the generated Rice mask but the sample sets of the rice field data is included. It is important to note that the NDVI differences of any other two image dates do not produce a reliable mask in the study area for separating Rice from the No-Rice area using the visual interpretation.

Figure 5-2 shows the overlay of the generated Rice, No-Rice mask with the colour composited images from different dates. As it is shown in the figure almost all the fields with the most changes in three images (period of rice growth stages) selected as rice area.

Figure 5-1: The location of sample data on the generated Rice mask using the NDVI differences

Two classes of rice types (i.e., Shiroudi and Tarom) and one class of Water shown in Red color polygones

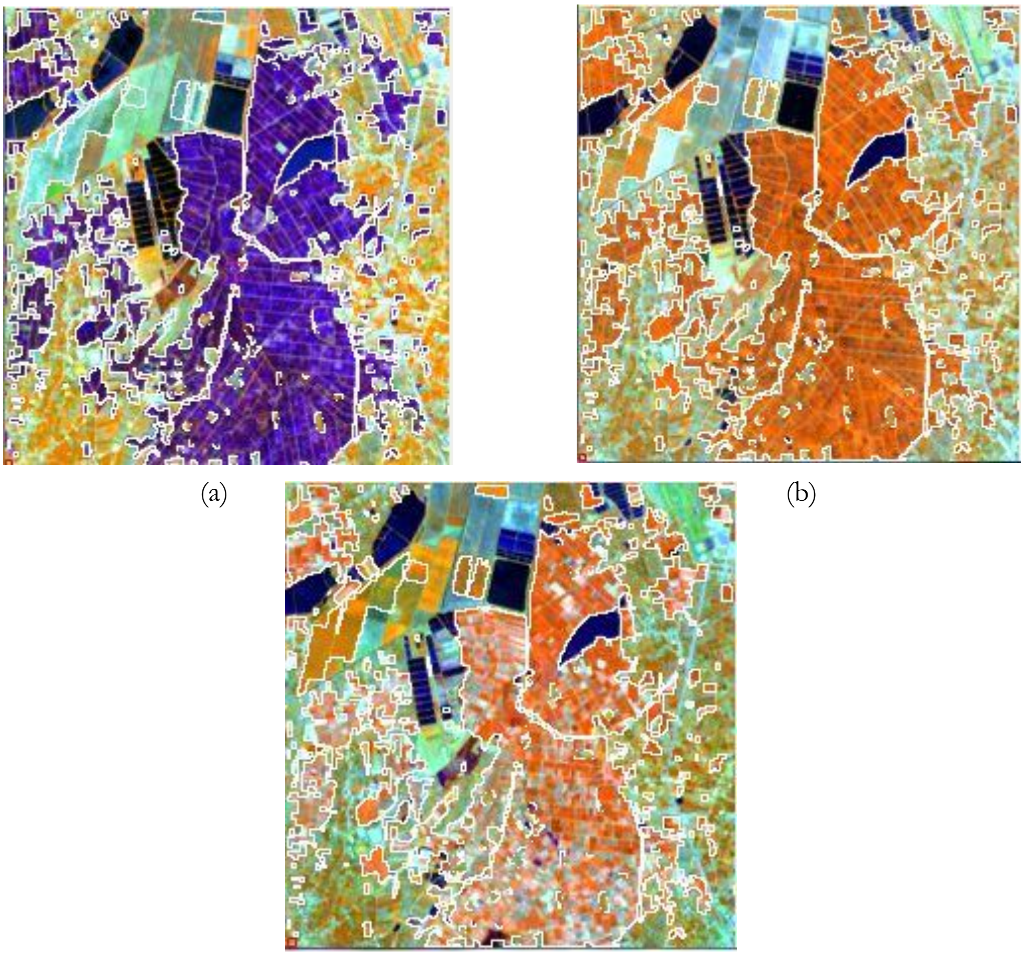

(a) (b)

(c)

Figure 5-2: Rice area selected from the generated Rice, No-Rice mask shown with White boundary superimposed on the color composites of the three image dates:

a) 27th May b) 14th July c) 15th August

According to the Table 5, the SVM method has better results with both input data (10 and 28 feature bands) over the RF method. From Table 5, the RF method using all the bands (28 bands) has the lowest kappa coefficient. Due to the low number of training samples in this study the kappa coefficient and overall accuracy are exaggerated. Table 7 shows the number of training samples in each class. (Pontius Jr et al. (2011)) concluded that kappa indices are misleading in classification accuracy assessment in remote sensing. The authors proposed two new indices named: quantity disagreement and allocation disagreement.

Table 7: Number of training samples for two rice types (Shiroudi and Tarom) and Water class

	Water	**Tarom**	**Shiroudi**
Number of training samples (pixel)	281	12	19
Number of polygons	2	2	2

By the visual comparison of the generated classification maps (Figure 4-6) and the generated colour composite images the following results can be achieved.

- Tarom as traditional varieties is already harvested on the 15th August. Satellite image of this date shows spectral changes in the bottom of the rice area and this area is classified as Tarom (red) in all the classification maps.
- The RF classification with 10 bands (Figure 4-6a) has not produced an acceptable result because it classified some parts of the rice area as water bodies, for which these areas are to be considered as the rice fields in three satellite images using visual interpretation. These areas are classified as Tarom in the rest of the classified maps.
- Existence of still some water bodies in the classified maps after applying the Rice mask could be attributed to the errors of the generated mask or the classification method.
- According to the Table 5 and Table 6, adding more feature bands could not necessarily increase the accuracy.

Feature space for the classes are plotted to check the spectral separability of two rice varieties in different bands. For each image date Green, Red and SWIR1 band plotted against the NIR band. Figure 5-3 shows the plotted training samples in these four bands for each image date. As it is depicted on the figure, training samples of two rice types (Tarom shown in red and Shiroudi shown in green) are stretched over the feature space of each band pair (NIR-RED, NIR-GREEN, NIR-SWIR1) in the first image date 27th May (Figure 5-3a, d, g). 14th July (middle of the growth stages) feature spaces (Figure 5-3b, e, h) shows better separability and a sort of formed clusters between the rice classes.
The mean and standard deviation of the classes for each band in all image dates are calculated and shown in Table 8. All the values are extracted from TOA reflectance bands.

Table 8: Statistics (mean and standard deviation) of three different classes training samples in the bands NIR, Green, Red and SWIR1

Band name	Image date	Mean			Standard deviation		
		Tarom	Shiroudi	Water	Tarom	Shiroudi	Water
NIR	27th May	12222.5	9895.1	6239.1	861.6	510.5	393.9
	14th July	19914.1	22695.3	6811.3	2070.1	1779.6	351.1
	15th August	17454.3	21670.5	6344.9	2870.05	1657.4	442.2
SWIR1	27th May	5590.6	3290.7	4052.1	1343.4	434.7	247.3
	14th July	8818.7	8538.05	3635.1	1152.1	517.8	208.4
	15th August	10600.5	8925.4	3270.7	1042.1	844.9	396.6
RED	27th May	7167.3	7444.1	7104.3	1478.7	596.1	1141.8
	14th July	5478.0	4393	5650.3	237.4	104.01	807.1
	15th August	7822.1	6046.8	5935.02	812.6	579.7	653.03
GREEN	27th May	7942.6	8114.1	8415.2	1097.4	351.9	1032.9
	14th July	7054.4	6058.5	6881.9	207.04	83.2	739.9
	15th August	8540.4	7328.6	7140.5	409.8	397.6	747.3

The effect of segmenting part before classification could be making more homogenous fields than the pixels. As the disease or other parameter like the weather conditions could affect the spectral values of a rice variety within a field, to some extent segmentation helps to keep the homogeneity of the fields by grouping all the pixels of each field in one object. It is important to note that finding the optimum segmentation parameters is a crucial point. The ideal results will be achieved when the generated objects fit the reality (in terms of geometry, i.e. size, shape etc.) in the best way. In other words, unreliable results will be achieved if segments become larger than the rice fields in addition too many small segments could also affect the classification results. In this research, it is tried to select optimum segmentation parameter but the effect of the different segmentation parameters or/and algorithms on the classification results must be tested in the future works.

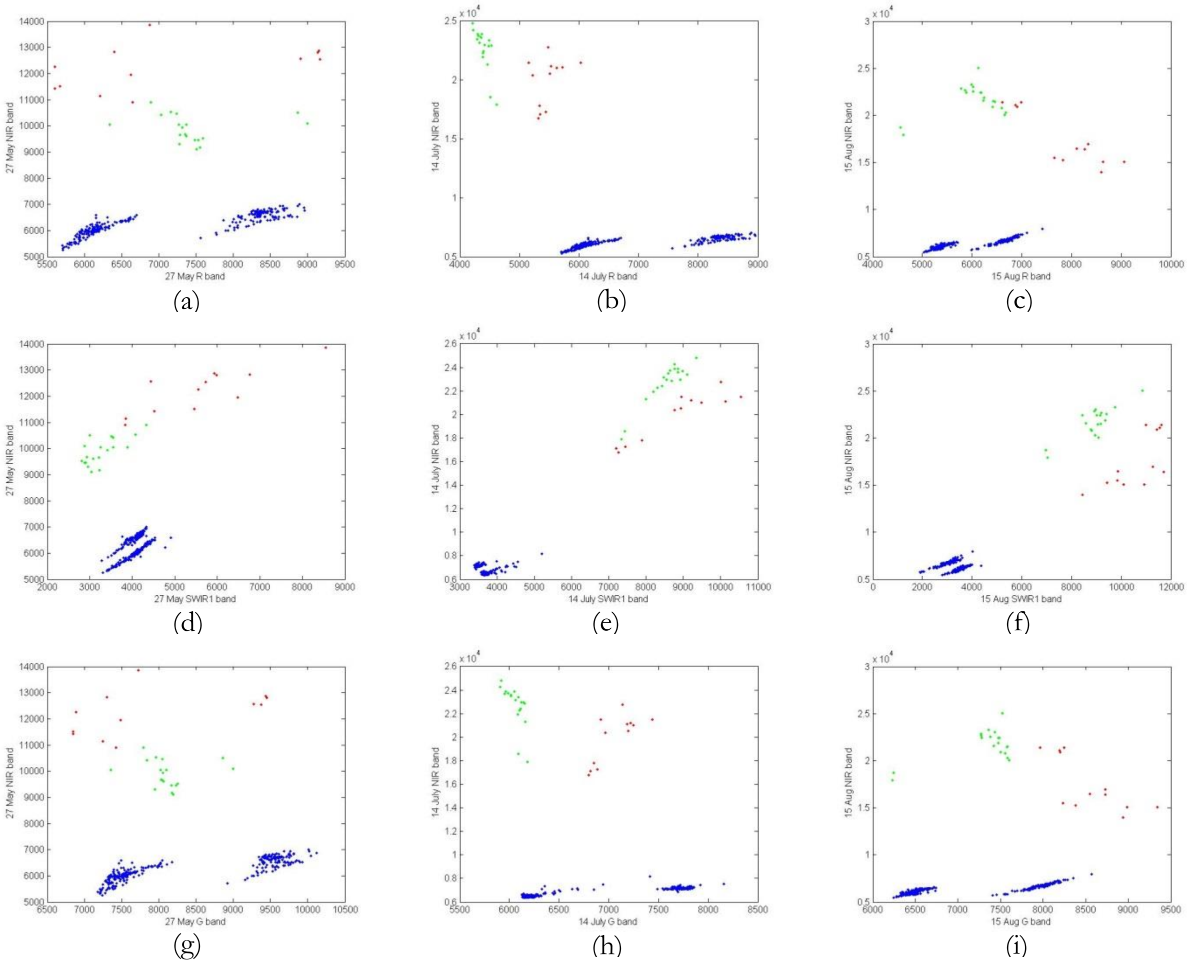

Figure 5-3: Feature space of three training sample sets

(a)-(c): feature space of two rice classes (Tarom shown in red and Shiroudi shown in green) and water class shown in blue for band NIR against R of the three image dates

(d)-(f): feature space of two rice classes (Tarom shown in red and Shiroudi shown in green) and water class shown in blue for band NIR against SWIR1 of the three image dates

(g)-(i): feature space of two rice classes (Tarom shown in red and Shiroudi shown in green) and water class shown in blue for band NIR against G of the three image dates

6. CONCLUSION AND RECOMMENDATIONS

6.1. Conclusion

This study was done to explore the possibility of classifying rice crop varieties using freely available source of multi-temporal satellite data like Landsat. In this section, the research questions are addressed:

1. Is it possible to classify traditional and high yielding rice varieties in the study area by use of multi-temporal satellite images?

Time as a dimension must be taken into account to investigate the agricultural field changes. It is especially important for rice as a crop with short growing time (less than 4 months in the study area). Traditional and high yielding rice varieties in the study area have almost similar spectral response in broad band satellite images but their differences during the growing stage is a good indicator to discriminate these varieties from each other.

2. How can local knowledge and additional information (e.g. crop calendar) be included in the multi-temporal image classification?

For generating the Rice mask in order to separate the Rice from No-Rice areas, information about the phenology of the rice varieties and crop calendar in the study area helped to find the best time of the crop NDVI changes for this purpose. Also, this information helps to select proper image dates. Although there are rice fields in the study area with size smaller than the Landsat pixel size, and as we have the knowledge about farmer trend to plant same varieties in an area, the classification of the varieties was possible using Landsat 8 satellite images.

3. Are Landsat 8 images proper (spectrally and spatially) to classify two main rice varieties in the regional level in the study area?

Landsat 8 products have two short-wave infrared bands and one NIR band. Due to the strong signals in the SWIR range in the flooding and transplanting time of rice cultivation period the Landsat 8 images has good spectral resolution to map rice paddies. This strong signal drop significantly as the rice canopy covers the background soil. In the varieties level, differences in the growing season caused changes in SWIR signal for the varieties that is harvested while the other varieties are still in the growing period.
Spatial resolution is not ideal because of the small size of rice fields in the study area but the farmers' practise to plant same varieties in an area helps to classify the varieties. Of course, some small fields with different varieties will be lost but this problem could be solved if an existing land use/cover map or higher resolution satellite images are used to extract the fields' boundaries first in the framework of knowledge-based or object-based classification algorithms.

6.2. Recommendations

This research was done to check the possibility of monitoring rice varieties by use of free multi-temporal Landsat 8 images in the study area. The main problem to reach this goal was the spatial resolution of these images. To solve this problem and improve the results, the following recommendations for further researches are addressed in this section.

- The segmentation part is the most important part of this research. To improve the results of the segmentation part, it is recommended to use at least one high resolution satellite image (with same date of other images acquisition) to extract the fields' boundaries.

- Using an automatic algorithm (e.g. RF) to optimize the feature selection part to find the best feature bands for the classification of the rice varieties.

- Due to the cloudy weather conditions in the study area some image dates were omitted from the classification. It is recommended to combine the optical satellite images with Synthetic Aperture Radar (SAR) data to improve the results.

- Using the existing data and/or knowledge contained in a GIS (e.g. existing roads and canals, land use/cover maps) in image analysis will help to improve the classification results and Rice mask generation. The help could be to select the training samples, to resolve the mixed boundary pixels, support the segmentation algorithm to segment the small rice fields compared to the Landsat 8 pixel size.

- It is recommended to find the Rice mask threshold automatically and to quantify the errors and have an evaluation method for the generated Rice, No-Rice mask.

- In order to improve the results, it is proposed to perform field work in the study area and monitor different rice growth stages and different rice crop varieties. Also take sample about No-Rice areas for further improvements of the results of classification and segmentation.

LIST OF REFERENCES

Bilgin, G., Erturk, S., Yildirim, T. (2011). Segmentation of hyperspectral images via subtractive clustering and cluster validation using one-class support vector machines. *Geoscience and Remote Sensing, IEEE Transactions on, 49*(8), 2936-2944.

Boser, B. E., Guyon, I. M., Vapnik, V. N. (1992). *A training algorithm for optimal margin classifiers.* Paper presented at the Proceedings of the fifth annual workshop on Computational learning theory.

Breiman, L. (1996). Bagging predictors. *Machine learning, 24*(2), 123-140.

Breiman, L. (2001). Random forests. *Machine learning, 45*(1), 5-32.

Breunig, F. M., Galvao, L. S., Formaggio, A. R., Epiphanio, J. C. N. (2011). Classification of soybean varieties using different techniques: case study with Hyperion and sensor spectral resolution simulations. *Journal of Applied Remote Sensing, 5*. doi: 10.1117/1.3604787

Dalponte, M., Bruzzone, L., Gianelle, D. (2008). Fusion of hyperspectral and LIDAR remote sensing data for classification of complex forest areas. *IEEE Transactions on Geoscience and Remote Sensing, 46*(5), 1416-1427.

Darvishsefat, A. A., Abbasi, M., Schaepman, M. E. (2011). Evaluation of Spectral Reflectance of Seven Iranian Rice Varieties Canopies. *Journal of Agricultural Science and Technology, 13*, 1091-1104.

Drăgut, L., Tiede, D., Levick, S. R. (2010). ESP: a tool to estimate scale parameter for multiresolution image segmentation of remotely sensed data. *International Journal of Geographical Information Science, 24*(6), 859-871. doi: 10.1080/13658810903174803

FAO. (2013). Food and Agricultural commodities production. Retrieved June 3, 2013, from http://faostat.fao.org/site/339/default.aspx

Foody, G. M., Mathur, A. (2004). A relative evaluation of multiclass image classification by support vector machines. *Geoscience and Remote Sensing, IEEE Transactions on, 42*(6), 1335-1343.

Garcia-Gutierrez, J., Gonçalves-Seco, L., Riquelme-Santos, J. C. (2011). Automatic environmental quality assessment for mixed-land zones using lidar and intelligent techniques. *Expert Systems with Applications, 38*(6), 6805-6813.

Gislason, P. O., Benediktsson, J. A., Sveinsson, J. R. (2006). Random forests for land cover classification. *Pattern Recognition Letters, 27*(4), 294-300.

Guo, L., Chehata, N., Mallet, C., Boukir, S. (2011). Relevance of airborne lidar and multispectral image data for urban scene classification using Random Forests. *ISPRS Journal of Photogrammetry and Remote Sensing, 66*(1), 56-66.

Han, J., Kamber, M., Pei, J. (2006). *Data mining: concepts and techniques*: Morgan kaufmann.

Hazell, P. B. R. (2009). The Asian Green Revolution. *International Food Policy Research Institute (IFPRI).*

Hsu, C.-W., Chang, C.-C., Lin, C.-J. (2003). A practical guide to support vector classification.

Huang, C., Davis, L., Townshend, J. (2002). An assessment of support vector machines for land cover classification. *International Journal of Remote Sensing, 23*(4), 725-749.

Jin, J. (2012). A Random Forest Based Method for Urban Land Cover Classification using LiDAR Data and Aerial Imagery.

Jones, T. G., Coops, N. C., Sharma, T. (2010). Assessing the utility of airborne hyperspectral and LiDAR data for species distribution mapping in the coastal Pacific Northwest, Canada. *Remote Sensing of Environment, 114*(12), 2841-2852.

Li, C.-H., Kuo, B.-C., Lin, C.-T., Huang, C.-S. (2012). A spatial–contextual support vector machine for remotely sensed image classification. *Geoscience and Remote Sensing, IEEE Transactions on, 50*(3), 784-799.

Mahour, M., Abkar, A. A. (2012). *Evaluation of Model Based Image Analysis of Remotely Sensed Data Using Support Vector Machine and Bayes' Theorem*. Paper presented at the The second International Conference and Exhibition on Mapping and spatial Information (ICMSI 2012) and 19th National Geomatics Conference, National Cartographic Center (NCC) of Iran.

Melgani, F., Bruzzone, L. (2004). Classification of hyperspectral remote sensing images with support vector machines. *Geoscience and Remote Sensing, IEEE Transactions on, 42*(8), 1778-1790.

Micijevic, E., Morfitt, R., Choate, M. (2011). *Landsat 8 on-orbit characterization and calibration system.*

Mountrakis, G., Im, J., Ogole, C. (2011). Support vector machines in remote sensing: A review. *ISPRS Journal of Photogrammetry and Remote Sensing, 66*(3), 247-259.

Moustakidis, S., Mallinis, G., Koutsias, N., Theocharis, J. B., Petridis, V. (2012). SVM-based fuzzy decision trees for classification of high spatial resolution remote sensing images. *Geoscience and Remote Sensing, IEEE Transactions on, 50*(1), 149-169.

Niennattrakul, V., Srisai, D., Ratanamahatana, C. A. (2012). Shape-based template matching for time series data. *Knowledge-Based Systems, 26*(0), 1-8. doi: http://dx.doi.org/10.1016/j.knosys.2011.04.015

Nikfar, M., Zoej, M. J. V., Mohammadzadeh, A., Mokhtarzade, M., Navabi, A. (2012). Optimization of multiresolution segmentation by using a genetic algorithm. *Journal of Applied Remote Sensing, 6*(1), 063592-063592.

Nuarsa, I., Nishio, F., Hongo, C. (2010). Development of the empirical model for rice field distribution mapping using multi-temporal landsat etm+ data: case study in bali indonesia.

Pal, M. (2005). Random forest classifier for remote sensing classification. *International Journal of Remote Sensing, 26*(1), 217-222.

Petitjean, F., Inglada, J., Gancarski, P. (2012a). Satellite Image Time Series Analysis Under Time Warping. *Ieee Transactions on Geoscience and Remote Sensing, 50*(8), 3081-3095. doi: 10.1109/tgrs.2011.2179050

Petitjean, F., Kurtz, C., Passat, N., Gançarski, P. (2012b). Spatio-temporal reasoning for the classification of satellite image time series. *Pattern Recognition Letters, 33*(13), 1805-1815. doi: http://dx.doi.org/10.1016/j.patrec.2012.06.009

Pontius Jr, R. G., Millones, M. (2011). Death to Kappa: birth of quantity disagreement and allocation disagreement for accuracy assessment. *International Journal of Remote Sensing, 32*(15), 4407-4429.

Rabe, A., van der Linden, S., Hostert, P. (2010). *Simplifying support vector machines for classification of hyperspectral imagery and selection of relevant features.* Paper presented at the Hyperspectral Image and Signal Processing: Evolution in Remote Sensing (WHISPERS), 2010 2nd Workshop on.

Salah, M., Trinder, J. (2010). Support vector machines based filtering of lidar data: a grid based method.

Savin, I., Baruth, B. (2009). Rice acreage estimation in Kalmykia based on MODIS NDVI. *Earth Research from Space.*

Shao, Y., Fan, X., Liu, H., Xiao, J., Ross, S., Brisco, B., Brown, R., Staples, G. (2001). Rice monitoring and production estimation using multitemporal RADARSAT. *Remote Sensing of Environment, 76*(3), 310-325.

Shobha Rani, N. (1998). The rice situation in Iran. *International Rice Commission Newsletter, 47*.

Smith, A. (2010). Image segmentation scale parameter optimization and land cover classification using the Random Forest algorithm. *Journal of Spatial Science, 55*(1), 69-79.

Thi Thu Ha, N. (2013). *Earth observation for rice crop monitoring and yield estimation : application of satellite data and physically based models to the Mekong Delta.* University of Twente Faculty of Geo-Information and Earth Observation (ITC), Enschede. Retrieved from http://www.itc.nl/library/papers_2013/phd/nguyenha.pdf

U.S. Geological Survey. (2013, 29/8/2013). Frequently Asked Questions about the Landsat Missions. Retrieved 23/11/2013, 2013, from http://landsat.usgs.gov/ESUN.php

USGS. (2013, 06/12/2013). Landsat 8 Data Now Available! Retrieved 23 August, 2013, from http://landsat.usgs.gov/LDCM_Landsat8.php

Van Niel, T. G., McVicar, T. R. (2004). Current and potential uses of optical remote sensing in rice-based irrigation systems: a review. *Australian Journal of Agricultural Research, 55*(2), 155-185. doi: 10.1071/ar03149

Wang, Y., Li, J. (2008). Feature-selection ability of the decision-tree algorithm and the impact of feature-selection/extraction on decision-tree results based on hyperspectral data. *International Journal of Remote Sensing, 29*(10), 2993-3010.

Wu, S. S., Qiu, X., Usery, E. L., Wang, L. (2009). Using geometrical, textural, and contextual information of land parcels for classification of detailed urban land use. *Annals of the Association of American Geographers, 99*(1), 76-98.

Wu, T. F., Lin, C. J., Weng, R. C. (2004). Probability estimates for multi-class classification by pairwise coupling. *Journal of Machine Learning Research, 5*(975-1005), 4.

Xiao, X., Boles, S., Frolking, S., Salas, W., Moore, B., Li, C., He, L., Zhao, R. (2002). Observation of flooding and rice transplanting of paddy rice fields at the site to landscape scales in China using VEGETATION sensor data. *International Journal of Remote Sensing, 23*(15), 3009-3022. doi: 10.1080/01431160110107734

Xiao, X., Boles, S., Liu, J., Zhuang, D., Frolking, S., Li, C., Salas, W., Moore Iii, B. (2005). Mapping paddy rice agriculture in southern China using multi-temporal MODIS images. *Remote Sensing of Environment, 95*(4), 480-492. doi: http://dx.doi.org/10.1016/j.rse.2004.12.009

Zhou, W., Troy, A. (2008). An object-oriented approach for analysing and characterizing urban landscape at the parcel level. *International Journal of Remote Sensing, 29*(11), 3119-3135. doi: 10.1080/01431160701469065